

NASA SAGE SBIR structural, thermal, optical performance (STOP) analysis correlation to wavefront error testing

Christine Buleri^a, Cameryn Yow^a, Janak Carey^a, Robert Damadeo^b, Alexander Halterman^a, Charles Hill^b, John Leckey^b, Alicia Maccarrone^a, Samantha Weiner^a, Shimshone Yacoby^a
^aQuartus Engineering, 9689 Towne Centre Drive, San Diego, CA 92121 USA; ^bNASA Langley Research Center, 1 Nasa Drive, Hampton, VA 23666 USA

ABSTRACT

In conjunction with the NASA LaRC SAGE IV Pathfinder team, Quartus has developed a small format near-diffraction limited telescope designed to package into a 6U CubeSat. The SAGE IV Pathfinder telescope utilizes analytical models and designs that can be leveraged to meet a broad range of scientific optical mission needs by creating a family of semi-custom small format space-borne optical systems. During the initial phases of a science mission, a systems engineering assessment can be performed to identify existing designs and analysis tools that can be leveraged to meet many key requirements. This would allow limited resources to then be focused on developing required new components, as opposed to designing the entire optical system from the bottom up. This accelerates technical readiness level (TRL) progression on semi-custom small format precision optical systems, reducing instrument costs, and achieving economy of scale typically not available on one-off science payloads.

The current SAGE SBIR Phase II is a research program utilizing a SAGE-like design for development of STOP analysis correlation methodologies. Wavefront error (WFE) is captured over a variety of temperature ranges for comparison to finite element model (FEM) predictions. The accuracy and repeatability of the WFE measurement process over temperature is reviewed. Best practices for accurate STOP analysis and WFE predictions are summarized including modeling parameters, material properties, and strength and distortion assessments.

Keywords: SAGE IV, SBIR, STOP, FEM, FEA, Correlation, WFE, Thermal Testing, Nastran, Zemax, SigFit

1. INTRODUCTION

The 2017 decadal survey called out a need to reduce mission costs for space-based earth observation. To help meet this need, Quartus Engineering Incorporated (Quartus) proposed a SBIR to leverage analytical models and existing opto-mechanical designs to increase TRL levels more quickly on CubeSats and small satellite platforms. It is common for technology to be leveraged from mission to mission, such as customizable CubeSat, small sat, or larger satellite buses. This is less common with precision optical subsystems, which are often designed from the ground up to meet the science needs of a mission. By using validated analytical tools, optical components, and subsystem designs, new missions can increase their TRL level more rapidly by reducing the amount of design/analysis iteration. This approach can lead to semi-custom precision optical systems for space applications, much in the same way spacecraft bus suppliers support the science community. This paper summarizes the scope of work conducted for a SBIR Phase II related to the NASA LaRC SAGE IV Pathfinder instrument. This SBIR validated the designs and analytical tools used to assess the SAGE IV Pathfinder telescope for structural, thermal, optical performance (STOP) analysis. As an outcome, these designs and analytical tools can be used to accelerate development and reduce costs of future NASA and other science missions. Many smaller instrument missions and organizations within the science community will be able to take science requirements and quickly design and build a flight worthy optical instrument at a significantly reduced development cost by utilizing validated STOP analysis predictions. This is done in industry for high volume components and systems, but this is not typically leveraged for low volume high precision space based optical systems.

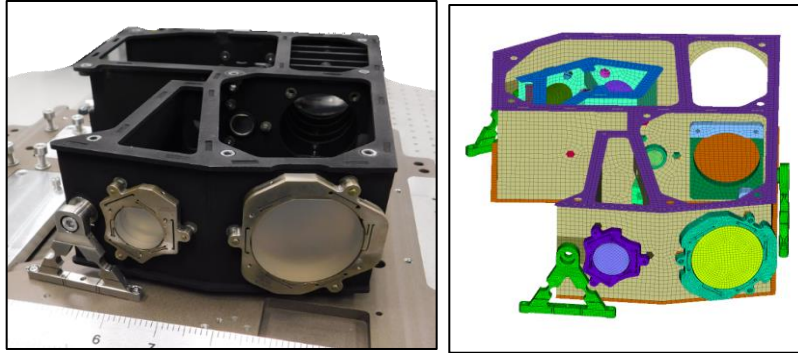


Figure 1-1: SAGE IV ground demonstration instrument (left) and detailed finite element model (right), designed, built, and analyzed by Quartus Engineering

2. SYSTEM LEVEL DESIGN, PRE-TEST ANALYSIS, AND TEST SETUP

2.1 System Level Design

In order to validate the Quartus STOP analysis modeling and methodology, a simplified “System Level Correlation” design was created from the original SAGE IV flight instrument design (Figure 1-1). With the low coefficient of thermal expansion (CTE) materials selected for the SAGE IV Pathfinder telescope, motion is expected to be very small, and within the noise of measured data. As such, the System Level Correlation assembly was designed to achieve appreciable motion such that the magnitudes could accurately and repeatably be measured. This increased motion allowed for more accurate correlation to the analytical model.

The metering structure for the System Level Correlation assembly was designed as a monolithic, metallic structure (Figure 2-1, Right). The base design was made from 6061-T6 Aluminum. The monolithic structure had the same profile as the SAGE-like carbon fiber structure, with the T1, T2 and T3 mounts all positioned in the same nominal locations. The field stop and the dividing wall that housed the field stop were not needed and were not added as part of this design. Zerodur optics and a combination of Invar and Stainless Steel optic mounts were used to intentionally induce higher stress and displacements within the optics.

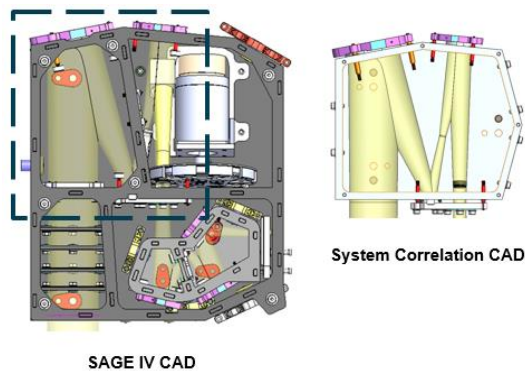


Figure 2-1: SAGE IV flight instrument (left) and System Level Correlation assembly CAD (right)

The base of the System Level Correlation assembly had tight-tolerance pads that served as the reference datum for assembly and alignment. The aluminum structure had both through holes and pin holes machined directly into the base for the build and inspection of the system. For temperature testing, spheres were threaded into the bottom and were used to kinematically mount the assembly in the thermal chamber.

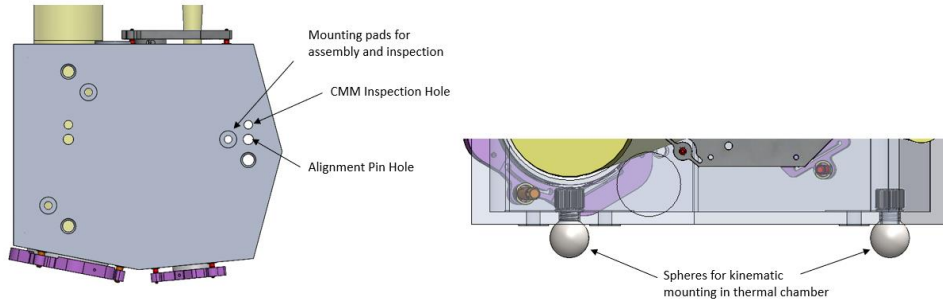


Figure 2-2: System Level Correlation assembly datum features and mounting

2.2 Test Setup & Validation

The test setup included the System Level Correlation assembly, ZYGO interferometer, thermal chamber, air current blocker, and fold mirrors on automated stages, as shown in Figure 2-3. The System Level Correlation assembly was mounted inside the thermal chamber and the ZYGO interferometer's beam was steered into the system. The main fold mirror was used to minimize tilt between the ZYGO and housing of the System Level Correlation assembly, and the retro mirror minimized tilt in the system's WFE.

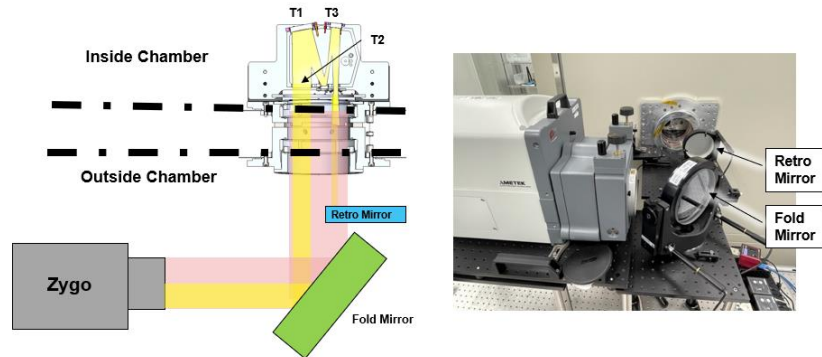


Figure 2-3: ZYGO to System Level Correlation assembly in thermal chamber setup

A large air current blocker was placed over the entire setup to help decrease air currents. After some initial testing, a more localized (smaller) air current blocker was added between the ZYGO and the thermal chamber window to help further decrease air currents, as shown in Figure 2-4. Testing was completed for repeatability and the noise floor of the testing setup including the thermal chamber window was determined to be $\leq 3\text{nm}$ RMS for WFE.



Figure 2-4: Small and large air current blockers used during data collection

2.3 Pre-test Analysis & FEM Overview

A detailed system-level FEM was analyzed for thermal distortion analysis in NX/NASTRAN [Ref. 1] for the System Level Correlation assembly. Figure 2-5 shows the correlation FEM, including the kinematic constraint at the tooling ball locations. This constraint uses beam elements that allow expansion or contraction of the assembly based on the CTE of the test plate. The correlation configuration uses a solid element representation of the Aluminum 6061-T6 bench to allow detailed modeling of the adhesive bond between the pressed-in sleeves representing the inserts and the Invar pins, described further below. Aluminum 6061-T6 was chosen to induce WFE in the target range for testing. To achieve positive strength margins of safety, the T2 mount material was updated from Invar (used for the SAGE-like configuration) to Stainless Steel 17-4PH H1150. SS 17-4PH has a similar Young's modulus as Invar, but has a higher yield strength than Invar. It has a CTE which is in between the CTE of the Aluminum 6061-T6 bench and the Zerodur optics. This allowed the T2 mount to still induce some amount of WFE, while keeping the strength margins for both the T2 Mount and the T2 Optic positive.

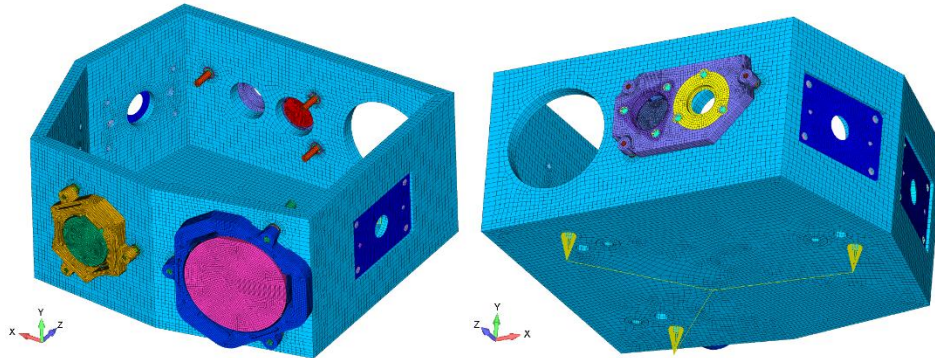


Figure 2-5: System-level Correlation FEM

For the correlation configuration, all adhesive bonds were modeled using 8-node linear solid elements (CHEXA) with three elements thru-thickness. Figure 2-6 shows a detailed view of the Hysol 9394 adhesive at the Pin-to-Bench interface and the Optic-to-Mount interface for the correlation configurations. To determine the adhesive allowable stresses, coupon FEM correlations of shear strength to specific element size were conducted.

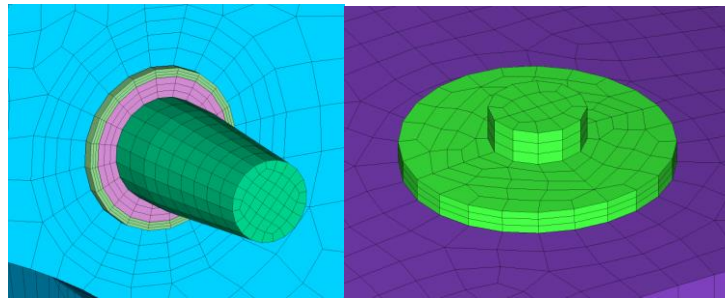


Figure 2-6: Pin-to-Bench Adhesive Bond (left) and Optic-to-Mount Adhesive Bond (right)

Material properties and strengths for Invar, Hysol 9394, Zerodur, SS 17-4PH and Aluminum 6061-T6 were implemented in the FEM and strength margins of safety were calculated. For Hysol 9394, temperature dependent material properties were based on testing performed by NTS in January 2022. For Zerodur, the ultimate strength was calculated using a Weibull distribution with a probability of failure of $1e-6$. Factors of safety used for the margins of safety comply with standards specified in GEVS: metallic yield = 1.25, metallic ultimate = 1.4, glass ultimate = 1.4, adhesive ultimate = 1.5. Additionally, microyield margins of safety were calculated using a factor of safety = 1.0 and an additional factor of safety of 1.25 was applied to the optic-to-mount adhesive bonds to account for variation in element size.

The thermoelastic analysis was split into three different temperature ranges based on the cold and hot survival temperatures, and the range where all margins of safety were positive. This analysis led to the definition of the “phases”

for testing. Phase 1 included the temperature range from 0°C to +40°C where the adhesive Hysol 9394 CTE remained linear and all margins of safety including microyield were positive, as shown in Table 2-2. Phases 2 and 3 refer to the cold survival (+20°C to -40°C) and hot survival (+20°C to +60°C) ranges, respectively. Ultimately, testing and correlation was only conducted on Phase 1 for the scope of the SBIR Phase II funding. However, Phases 2 & 3 may be revisited during a future SBIR or under internal funding provided by Quartus.

Displacements in microns for Phase 1 (0°C shown, 40°C is identical due to linear FEM) are shown in Figure 2-7. SigFit [Ref. 2] was used to convert the FEM nodal displacements to a Zemax .zpl macro that includes Zernike coefficients and rigid body motions. WFE error within Zemax [Ref. 3] was then calculated for the full system as shown in Figure 2-8 and Table 2-1. The WFE target and objective for the correlation FEM were 40 nm RMS and 80 nm RMS, respectively. The Phase 1 (0°C to +40°C) values were 5x/10x the SAGE IV nominal flight system WFE budget for environmental effects of 8 nm RMS. The current correlation FEM/Zemax prediction for WFE was 143 nm RMS for the Phase 1 cold case (0°C) and 143 nm RMS for the Phase 1 hot case (+40°C), which both meet the established target and objective values. The primary aberration in the system was defocus, which was driven by the piston displacement between mirrors. The secondary aberration was astigmatism caused by the tilts and decenters of the mirrors.

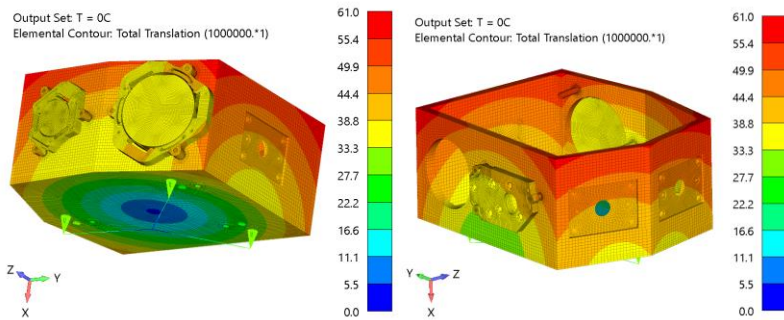


Figure 2-7: Correlation System Phase 1 (0°C to +40°C) Displacements [microns]

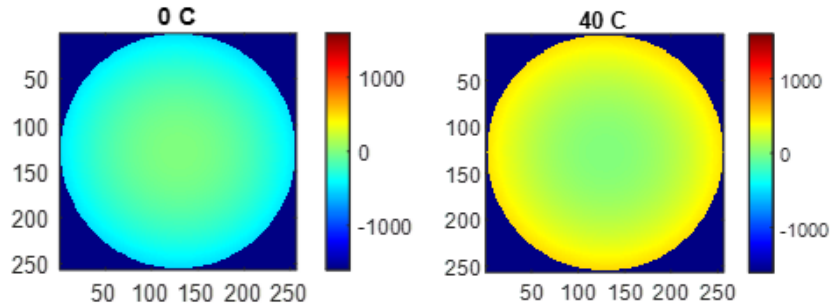


Figure 2-8: Correlation System Phase 1 (0°C to +40°C) Normalized WFE

	WFE (nm)	PV	RMS
Phase 2	-40C	1551	431
	-20C	1034	287
	-10C	775	215
Phase 1	0C	517	143
	10C	258	72
Phase 3	20C	0	0
	30C	258	72
	40C	517	143
	50C	775	215
	60C	1034	287

Table 2-1: Correlation System Phase 1-3 Normalized WFE

Strength margins of safety were calculated for all components in the Correlation FEM. The metallic components' von Mises stresses were compared to the material yield, ultimate, and microyield strengths and factors of safety as described above. The optics' maximum principal stresses were compared to a calculated Weibull allowable assuming a failure probability of 1e-6 and include a factor of safety of 1.4. In order to determine the adhesive allowable stresses, coupon FEM correlation of shear strength to specific element size was conducted for each of the six bonds. Stresses in the system FEM were then compared to the derived correlated adhesive allowable and include a factor of safety of 1.5. For the optic to mount adhesive bonds, an additional uncertainty factor of 1.25 was applied to account for the small differences in element size that will affect the stress values. The Pin-to-Bench adhesive bond element sizes are uniform, so this factor was not included. Metallic parts modeled with solids utilize shellcoat von Mises elemental max without corner data, adhesives utilize solid von Mises elemental max with corner data, and optics utilize shellcoat maximum principal or maximum shear stress without corner data.

All margins of safety were positive for Phase 1 (0°C to +40°C) as shown in the summary in Table 2-2. The minimum margin of safety is +0.06 and occurs at a large radius in the T1 Mount as shown in Figure 2-9. The next lowest margins occur in the T3 Mount (+0.24, Figure 2-9) and the margins of safety for the optics and adhesive remained positive even at the hot or cold survival temperatures of Phases 2 & 3. Stress contour plots are shown in Figure 2-9 for the optic mounts, Figure 2-10 for the optics, Figure 2-11 for the adhesive bonds.

Component	Material	Allowable [MPa]			Cold Case (0°C)				Hot Case (+40°C)			
		Yield	Ultimate	Microyield	Stress (MPa)	Yield MS	Ultimate MS	Microyield MS	Stress (MPa)	Yield MS	Ultimate MS	Microyield MS
Optic Bench	Aluminum 6061-T6	241	-	127	19.7	8.8	-	5.5	19.7	8.8	-	5.5
T1 Mount	Invar 36	276	-	75	70.7	2.1	-	0.06	70.7	2.1	-	0.06
T2 Mount	SS 17-4PH H1150	724	-	145	98.0	4.9	-	0.48	98.0	4.9	-	0.48
T3 Mount	Invar 36	276	-	75	60.6	2.6	-	0.24	60.6	2.6	-	0.24
T1 Sleeves	Aluminum 6061-T6	241	-	127	29.7	5.5	-	3.3	29.7	5.5	-	3.3
T2 Sleeves	Aluminum 6061-T6	241	-	127	38.9	4.0	-	2.3	38.9	4.0	-	2.3
T3 Sleeves	Aluminum 6061-T6	241	-	127	30.6	5.3	-	3.1	30.6	5.3	-	3.1
T1 Pins	Invar 36	276	-	75	50.0	3.4	-	0.50	50.0	3.4	-	0.50
T2 Pins	SS 17-4PH H1150	724	-	145	66.9	7.7	-	1.2	66.9	7.7	-	1.2
T3 Pins	Invar 36	276	-	75	54.5	3.1	-	0.38	54.5	3.1	-	0.38
T1 Optic	Zerodur	-	21	-	1.5	-	9.1	-	2.2	-	5.9	-
T2 Optic	Zerodur	-	21	-	3.1	-	3.9	-	5.0	-	2.0	-
T3 Optic	Zerodur	-	21	-	1.9	-	7.0	-	2.8	-	4.4	-
T1 Optic-to-Mount Adhesive	Hysol 9394	-	164	-	19.7	-	3.4	-	19.7	-	3.4	-
	Zerodur	-	21	-	2.7	-	4.6	-	2.8	-	4.4	-
T2 Optic-to-Mount Adhesive	Hysol 9394	-	227	-	18.4	-	5.6	-	18.4	-	5.6	-
	Zerodur	-	21	-	4.2	-	2.6	-	5.8	-	1.6	-
T3 Optic-to-Mount Adhesive	Hysol 9394	-	184	-	20.8	-	3.7	-	20.8	-	3.7	-
	Zerodur	-	21	-	4.6	-	2.3	-	3.2	-	3.7	-
T1 Pin-to-Bench Adhesive	Hysol 9394	-	145	-	26.1	-	2.7	-	26.1	-	2.7	-
T2 Pin-to-Bench Adhesive	Hysol 9394	-	145	-	24.9	-	2.9	-	24.9	-	2.9	-
T3 Pin-to-Bench Adhesive	Hysol 9394	-	145	-	24.7	-	2.9	-	24.7	-	2.9	-
T2 Optic Cover	Aluminum 6061-T6	241	-	127	2.0	>10	-	>10	2.0	>10	-	>10
Lyot Stop Aperture	Aluminum 6061-T6	241	-	127	2.0	>10	-	>10	2.0	>10	-	>10
Bipod Plates	Aluminum 6061-T6	241	-	127	0.6	>10	-	>10	0.6	>10	-	>10

Table 2-2: Correlation System Phase 1 (0°C to +40°C) Strength Margins of Safety

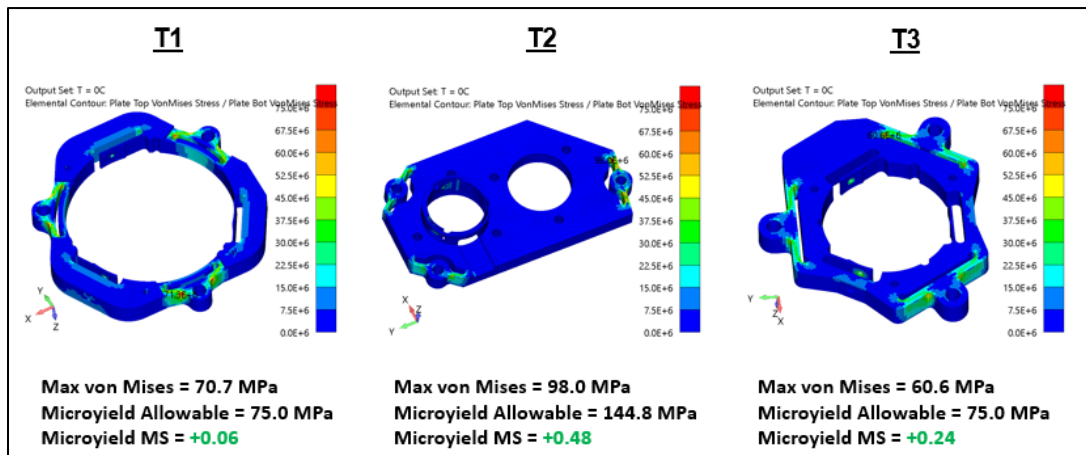


Figure 2-9: Correlation System Phase 1 (0°C to +40°C) Optic Mount Stress Contours

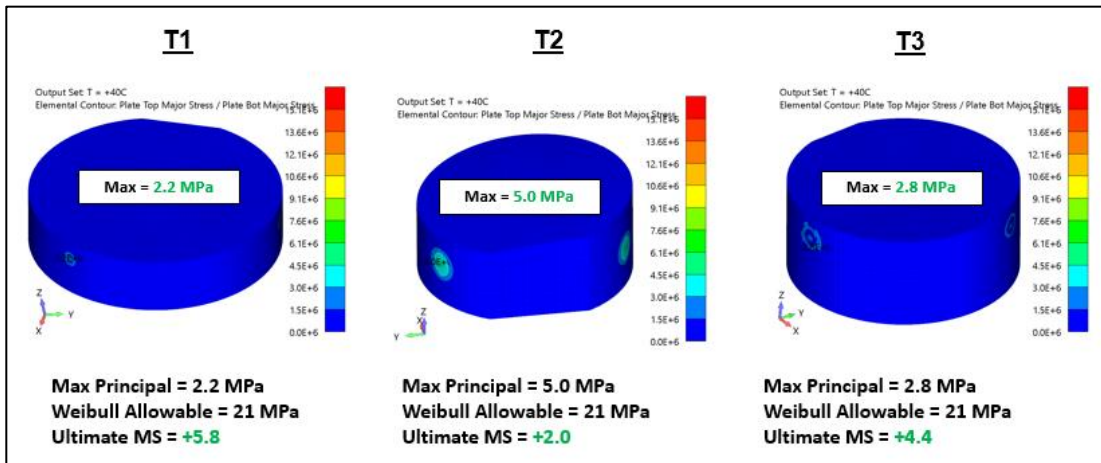


Figure 2-10: Correlation System Phase 1 (0°C to +40°C) Optic Stress Contours

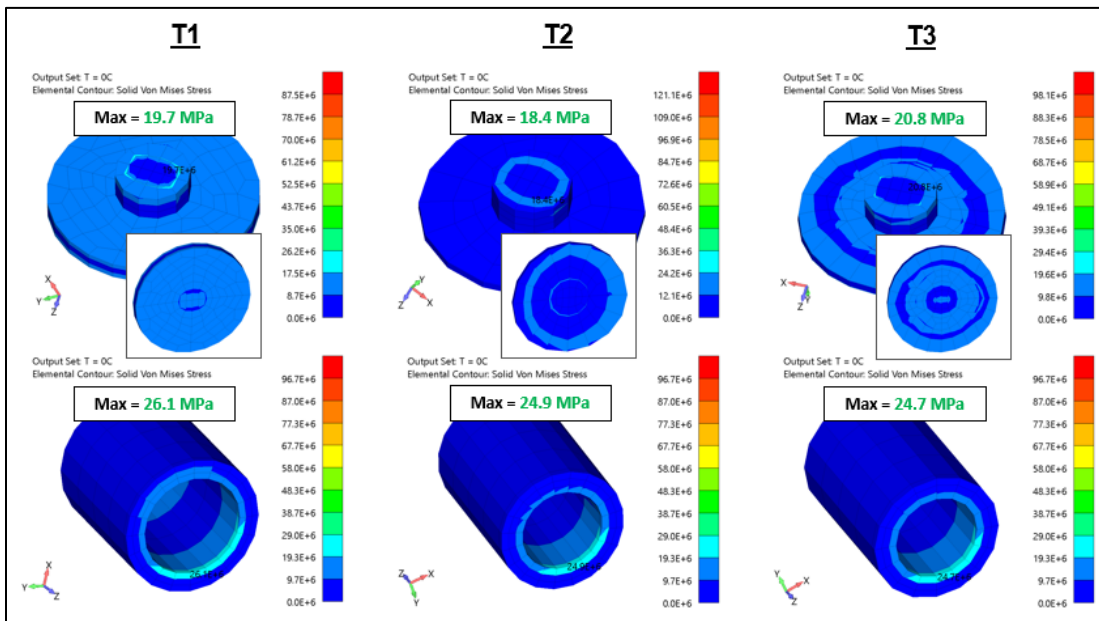


Figure 2-11: Correlation System Phase 1 (0°C to +40°C) Adhesive Bonds Stress Contours

3. WAVEFRONT ERROR TESTING

3.1 Test Plan

Using lessons learned from the NTS adhesive testing and the glass transition temperature of the adhesive, the System Level Correlation assembly was tested in cycles. The testing focused on Phase 1 (0°C to +40°C) where the adhesive Hysol 9394 CTE remains linear and all margins of safety including microyield are positive. Phase 1 was further divided into Phase 1A and Phase 1B, as outlined in Figure 3-1 in order to increase the temperature delta in an iterative fashion.

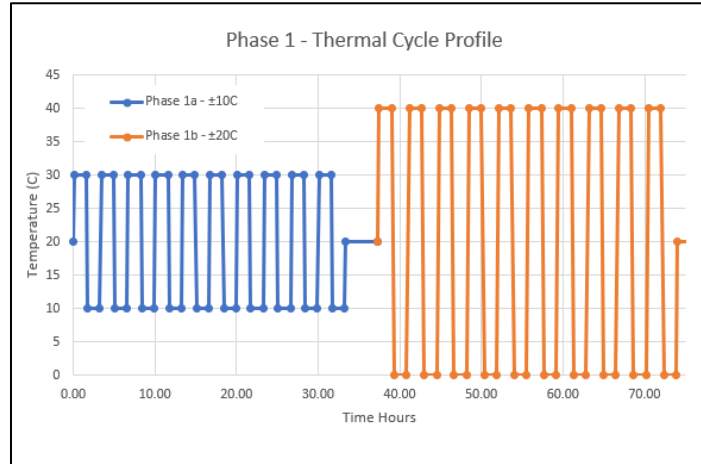


Figure 3-1: Phase 1 thermal cycle profile. Blue portion is Phase 1A and the orange portion of the image is Phase 1B.

Phase 1A cycles 1-5 moved through 10°C to 30°C in 10°C increments with a 90-minute soak time at each temperature. After reviewing the first five cycles of data it was decided that a longer soak time at the lower temperatures provided more stable results. Therefore, Phase 1A cycles 6-10 moved through 10°C to 30°C in 10°C, but with a 120-minute soak time at 10°C and 20°C and a 90-minute soak time at 30°C. Phase 1B cycles 1-5 moved through 0°C to 40°C with 20°C increments and 120-minute soak time at all temperatures. For all cycles, temperature, double-pass WFE out of T1, tilt on the back side of T2, input fold mirror tilt, and T3 return fold mirror tilt values were collected. Data review and success criteria for a phase occurred after every five cycles to review WFE for repeatability and comparison to FEM results. The requirement for WFE RMS at maximum and minimum temperatures for the cycles was to have <5-10% (target/objective) change from the average WFE RMS. If this target/objective was not met, then additional cycles were required. Within the final sub-phase, if the maximum and minimum temperatures were <5-10% (T/O) change from average WFE RMS, the phase was considered complete. At 20°C RMS WFE the success criteria was that the RMS WFE shall be less than 10nm to proceed, which was within the magnitude of our measurement resolution. If the RMS WFE at 20°C was greater than 10nm, then additional cycles were required before moving to the next phase. For the final sub-phase of 20°C, if the WFE RMS was <10% change or <10nm RMS from initial, then the phase was considered survivable and complete.

3.2 Test Results & Initial Comparison to FEM

For all results shown below the system WFE at 20°C and thermal chamber window WFE were subtracted from the measured result. A 90% clear aperture was also applied to the WFE plots. This was done to remove edge effects which would not affect the overall system performance. The FEM starting parameters assumed the system WFE to be 0nm and did not include the thermal chamber windows in its analysis.

Phase 1A cycles 1-5 data is shown in Table 3-1 and Figure 3-1 for the 90-minute measured data points. All data is reported in single pass and units are in nm.

Average System WFE at 20C Subtracted, thermal window error subtracted, Cropped to 90%								
		Avg (nm)	Min (nm)	Max (nm)	% Diff (min)	% Diff (max)	5% of avg (nm)	Meets Criteria
10C	PV	317	288	333	9.1%	5.2%	16	Pass
	RMS	73	68	75	6.3%	4.0%	4	Marginal
20C	PV	38	33	46	12.6%	21.2%	2	Pass
	RMS	5	3	6	26.5%	28.7%	0	Pass
30C	PV	318	302	330	4.9%	3.8%	16	Pass
	RMS	74	72	75	1.8%	1.9%	4	Pass

Difference > 10%
10% < Difference > 5%
Difference < 5%

Table 3-1: Phase 1A Cycles 1-5 Results

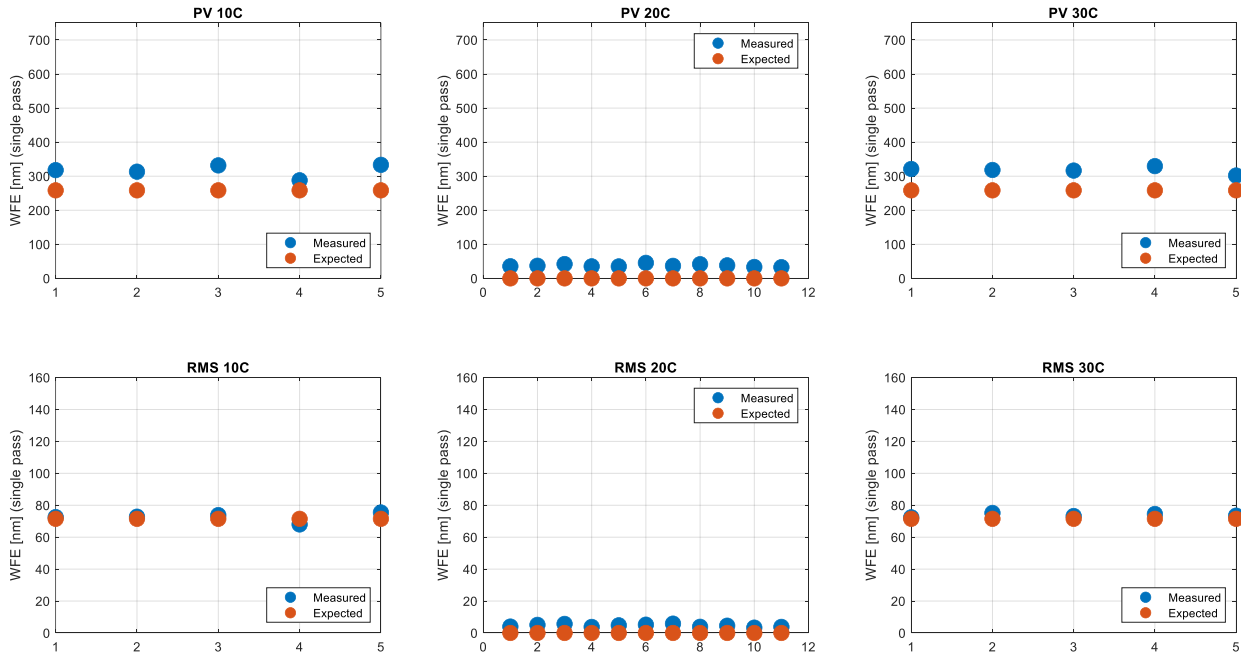


Figure 3-1: Phase 1A cycle 1-5 WFE plots. Orange data points are the expected RMS WFE predicted from FEM and blue data points are the measured RMS WFE. Results are for single pass and units are nm.

Phase 1A cycles 1-5 met the objective for success criteria, but it was decided to try a longer soak time to see if the target goal could be met for 10°C and 20°C.

Phase 1A cycles 6-10 data is shown in Table 3-2 and Figure 3-2 for the 120-minute measured data point for 10°C and 20°C, and the 90-minute measured data point for 30°C. All data is reported in single pass and units are in nm. Increasing soak time for Phase 1A cycles 6-10 increased the WFE repeatability and the target goal was met for all temperatures. WFE plots for Phase 1A cycles 1-10 are shown in Figure 3-3.

Average System WFE at 20C Subtracted, thermal window error subtracted, Cropped to 90%								
		Avg (nm)	Min (nm)	Max (nm)	% Diff (min)	% Diff (max)	5% of avg (nm)	Meets Criteria
10C	PV	322	306	334	5.0%	3.8%	16	Pass
	RMS	74	72	77	2.9%	3.8%	4	Pass
20C	PV	32	24	41	23.8%	30.8%	2	Pass
	RMS	4	3	6	27.0%	60.0%	0	Pass
30C	PV	312	299	331	4.1%	6.2%	16	Pass
	RMS	74	72	77	2.7%	4.4%	4	Pass

Difference > 10%
10% < Difference > 5%
Difference < 5%

Table 3-2: Phase 1A Cycles 6-10 Results

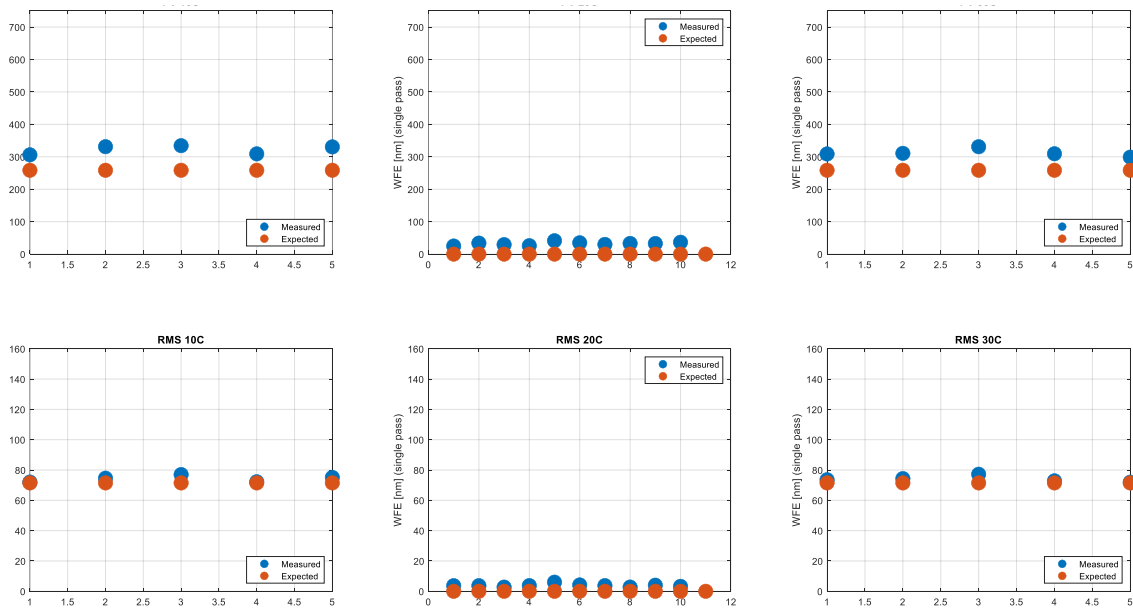


Figure 3-2: Phase 1A cycle 6-10 WFE plots. Orange data points are the expected RMS WFE predicted from FEM and blue data points are the measured RMS WFE. Results are for single pass and units are in nm.

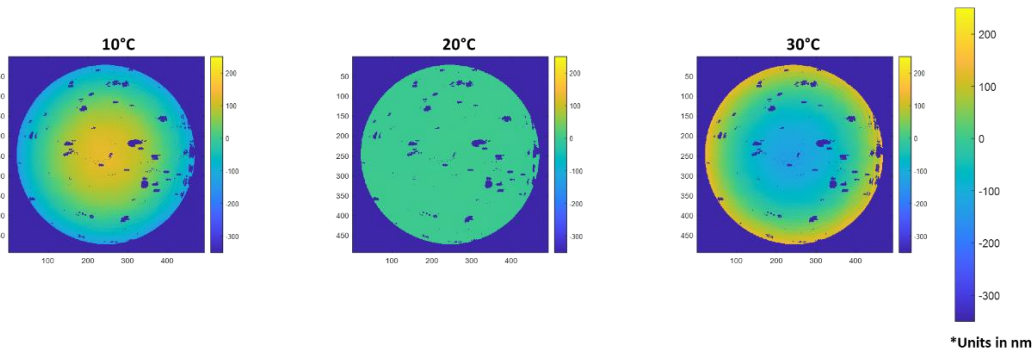


Figure 3-3: Phase 1A average WFE plots for cycles 1-10. System WFE and thermal chamber window WFE is subtracted. A 90% clear aperture is applied. Units are in nm.

Phase 1B cycles 1-5 data is shown in Table 3-3 and Figure 3-4 for the 120-minute measured data point. All data is reported in single pass and units are in nm. WFE plots for Phase 1B cycles 1-5 are shown in Figure 3-5. Phase 1B cycles 1-5 met the target for success criteria so no additional cycles were required.

Average System WFE at 20C Subtracted, thermal window error subtracted, Cropped to 90%								
		Avg (nm)	Min (nm)	Max (nm)	% Diff (min)	% Diff (max)	5% of avg (nm)	Meets Criteria
0C	PV	606	596	614	1.8%	1.2%	30	Pass
	RMS	139	138	141	0.7%	1.5%	7	Pass
20C	PV	47	32	70	30.7%	48.3%	2	Pass
	RMS	4	3	7	36.6%	74.6%	0	Pass
40C	PV	610	576	628	5.5%	3.0%	31	Pass
	RMS	147	142	149	3.2%	1.3%	7	Pass

Difference > 10%
10% < Difference > 5%
Difference < 5%

Table 3-3: Phase 1B Cycles 1-5 Results

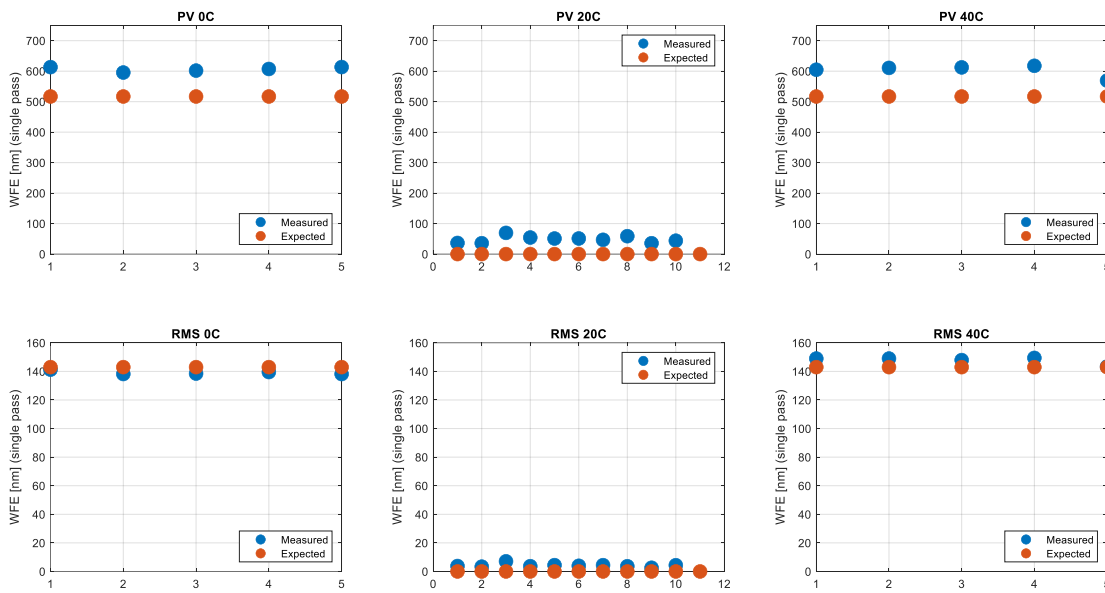


Figure 3-4: Phase 1B cycle 1-5 WFE plots. Orange data points are the expected RMS WFE predicted from FEM and blue data points are the measured RMS WFE. Results are for single pass and units are nm.

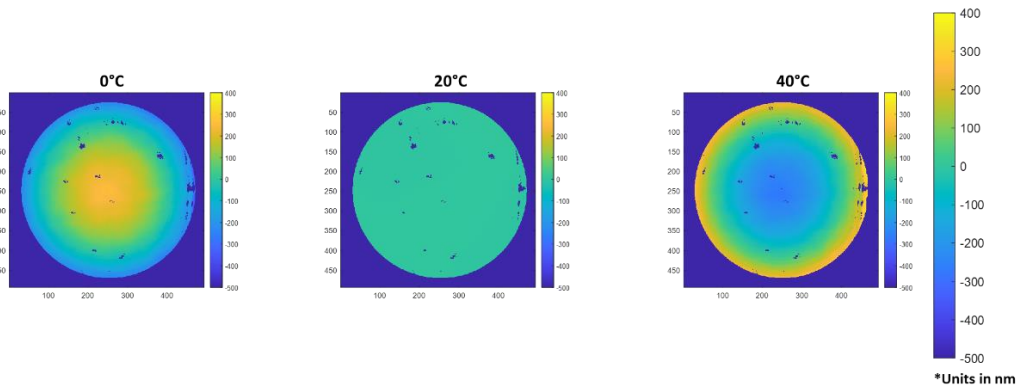


Figure 3-5: Phase 1B average WFE plots for cycles 1-5. System WFE and thermal chamber window WFE is subtracted. A 90% clear aperture is applied. Units are in nm.

4. FEM CORRELATION

4.1 Trade Study 1 Results

Trade #1 examined the effect of updating the liquid pin joint from a complete solid brick mesh to a shell/beam/spring representation as shown in Figure 4-1. A shell/beam/spring modeling approach is more common for FEMs used for dynamic analysis and later updated for thermal distortion. If this approach can show similar WFE as the solid brick mesh, STOP analysis could be conducted in a fraction of the time as is typically required for a solid STOP analysis mesh. A variety of options of beam and spring stiffness as well as length of the beam representing the liquid pin itself were completed. The variation that best matched the test data and solid pre-test FEM included a beam element that modeled the unconstrained length of the pin only (i.e. the portion of the pin that is pressed into the mount was not modeled). This can be seen in the inset image in Figure 4-1. Global displacements as well as displacements on the optics and mounts match very closely as shown in Figure 4-2 and Figure 4-3. WFE from this variation matches test data within 1% on RMS and 16% on P-V as seen in Table 4-1.

Stresses within the optic mounts varied from 1% (T1) up to 14% (T3) as shown in Table 4-2 and seen in closer detail for the mounts of T1, T2, and T3 in Figure 4-4, Figure 4-5, and Figure 4-6, respectively. Margins of safety for the optic mounts were low for microyield (min MS = +0.06) so care must be taken to ensure stresses remain conservative. Even though stresses in the optics themselves were low and margins of safety remained high (min MS glass = +2.0) in this trade, the same care is recommended due to uncertainty in glass materials when switching to a coarser modeling approach. For a coarser shell/beam/spring representation, it is recommended to include an uncertainty factor on stresses of 20% to ensure any margins of safety are conservative.

It is worth noting that this trade was conducted on the single design from this SBIR for uniform temperatures and that this approach is not recommended broadly to all designs or even all load cases for the same design. Additionally, assessing strength in the liquid pin joint itself using this type of modeling requires test data for failure loads of the joint under temperature – which may be hard to come by. However, given these caveats, this approach is valid for STOP analysis at the concept level for early program trade studies at a minimum. If failure load allowables for the liquid pin insert assemblies under temperature extremes can be determined, then this approach becomes more feasible for later phases of analysis as well.

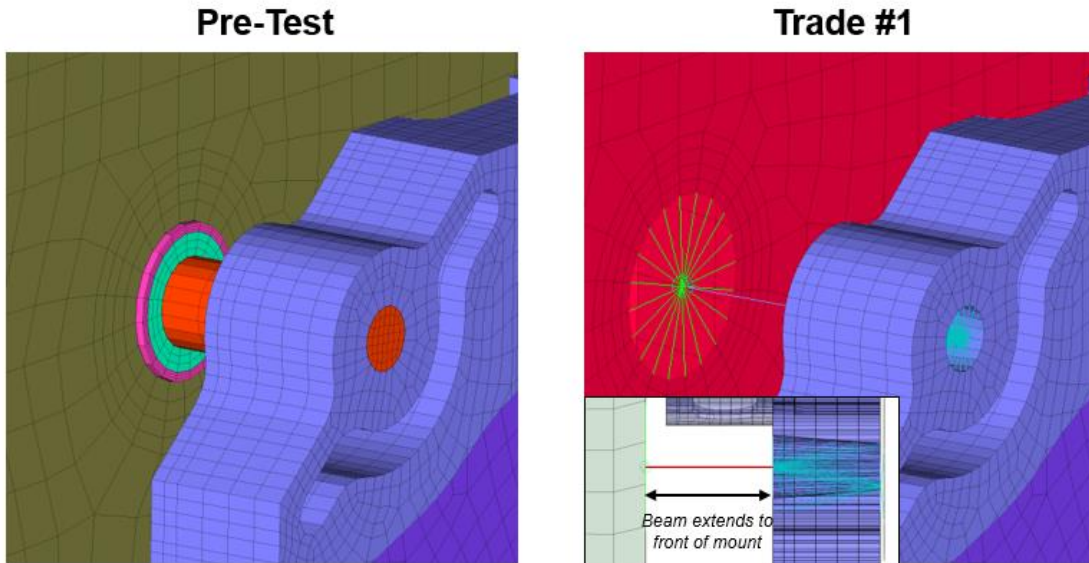


Figure 4-1. Meshing Approach for Pre-test (left) and Trade #1 (right)

Trade	WFE											
	0°C				40°C				0°C & 40°C Average			
	PV		RMS		PV		RMS		PV		RMS	
	[waves]	[nm]	[waves]	[nm]	[waves]	[nm]	[waves]	[nm]	[nm]	% Diff.	[nm]	% Diff.
Test Data	-	606	-	139	-	610	-	147	608	-	143	-
Pre-Test	1.0255	520	0.2814	143	1.0139	514	0.2813	143	517	-15.0%	143	-0.2%
Trade #1	1.0158	515	0.2790	141	1.0041	509	0.2789	141	512	-15.8%	141	-1.0%

Table 4-1. Trade #1 WFE Comparison

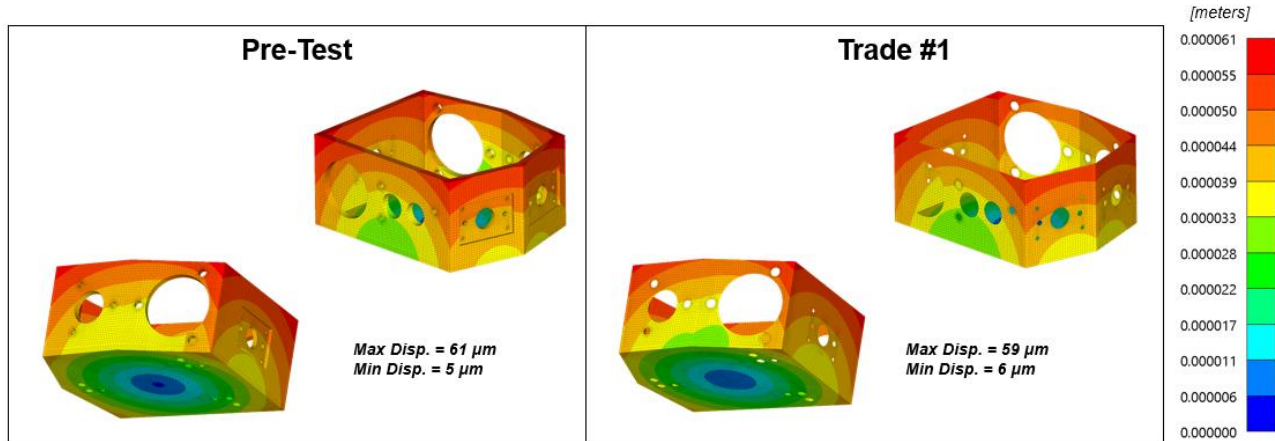


Figure 4-2. Global Displacements for Pre-test (left) and Trade #1 (right)

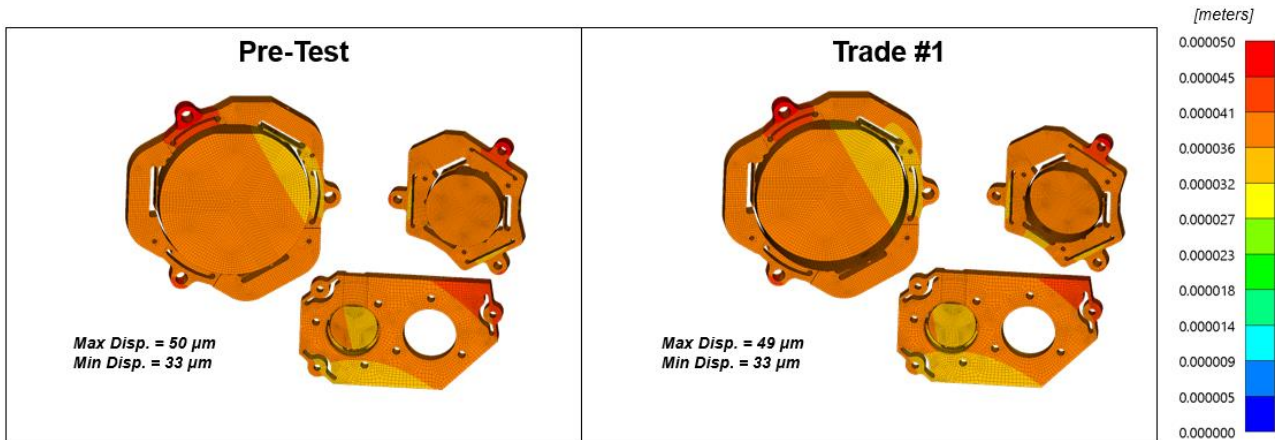


Figure 4-3. Optic & Mount Displacements for Pre-test (left) and Trade #1 (right)

Trade	Mounts								
	Max Stress [MPa]			Min Microyield MS			Stress % Diff. from Pre-Test		
	T1	T2	T3	T1	T2	T3	T1	T2	T3
Pre-Test	70.7	98.0	60.6	0.06	0.48	0.24	-	-	-
Trade #1	69.7	87.6	52.3	0.08	0.65	0.43	-1%	-11%	-14%

Table 4-2. Trade #1 Optic Mount Stress Comparison

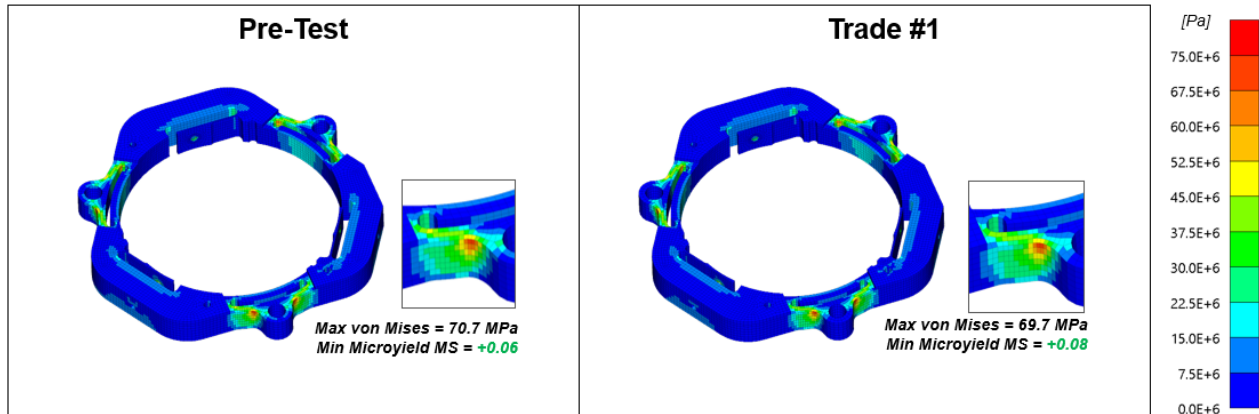


Figure 4-4. T1 Mount Stress for Pre-test (left) and Trade #1 (right)

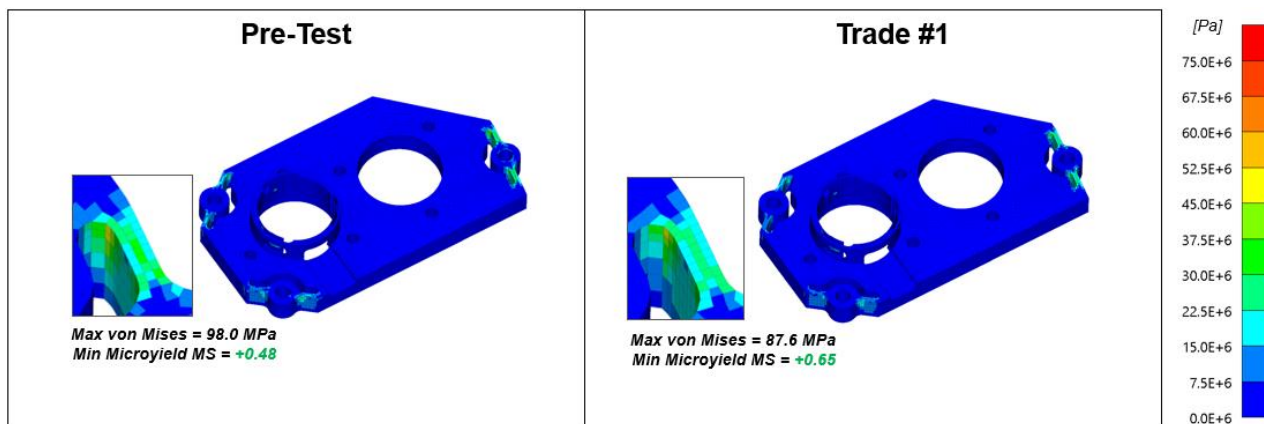


Figure 4-5. T2 Mount Stress for Pre-test (left) and Trade #1 (right)

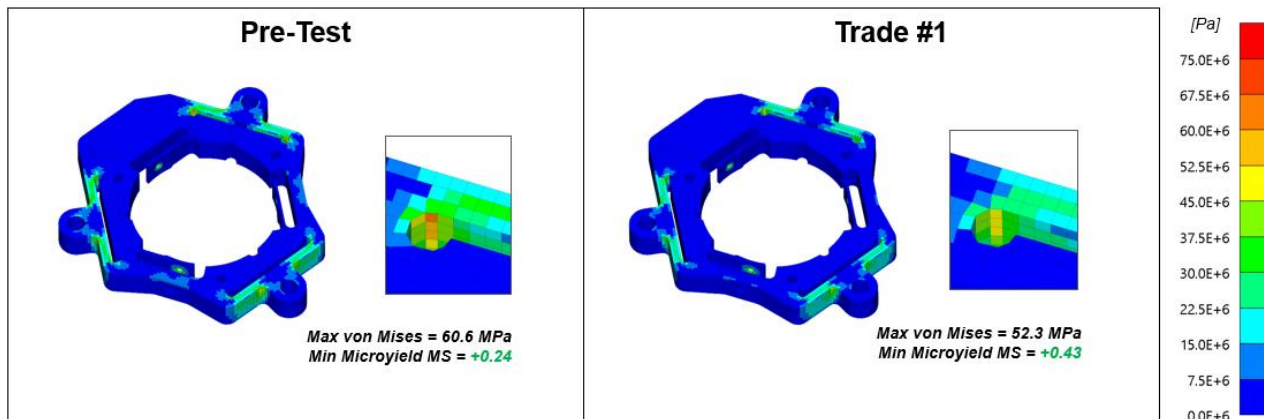


Figure 4-6. T3 Mount Stress for Pre-test (left) and Trade #1 (right)

4.2 Trade Study 2 Results

Trade #2 examined the effect of optic and optic-to-mount adhesive mesh size, connections, and element type on the resulting WFE and stresses. For the adhesive, a coarser parabolic tetrahedral mesh with glued contact and a beam/spring representation were included as options. For the optic, a coarser parabolic tetrahedral mesh with and without an explicit mesh split line at the clear aperture was included as an option. Images of the various mesh types and sizes are shown below in Figure 4-7.

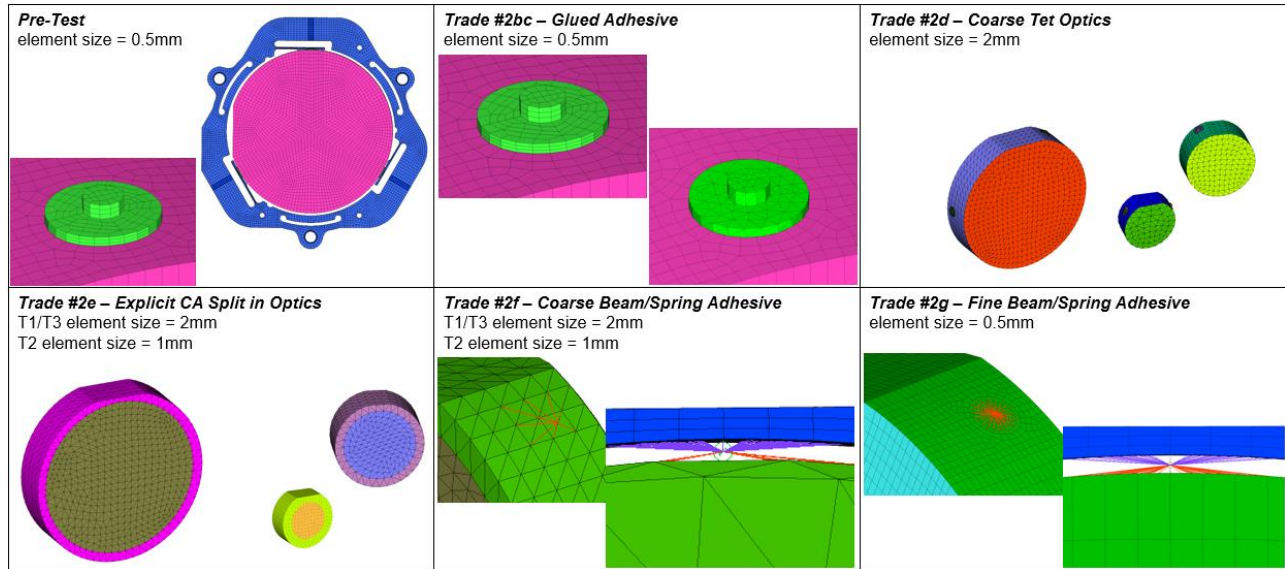


Figure 4-7. Trade #2 Mesh Sizes, Types, and Connections

Since the WFE of the System Level Correlation assembly is primarily driven by de-spacing between optics due to aluminum bench CTE, there is very little effect on WFE (RMS or P-V) for any combinations of solid optic and solid adhesive (glued, merged, CHEX8/brick, CTETRA10/parabolic tet) or explicitly meshed clear aperture vs. aperture applied in SigFit as seen in Table 4-3 and Figure 4-8 for Trades #2abcde. However, Trades #2fg (Beam/Spring Adhesive) showed larger changes in WFE values and an altered WFE shape as well. Additionally, when examining the surface figure error for individual optics, small changes were visible even among Trades #2abcde with very large changes qualitatively in Trades #2fg, as seen in Figure 4-9, Figure 4-10, and Figure 4-11, for T1, T2, and T3 respectively. However, modeling the adhesive joint with stiff beam/spring elements provided RMS WFE within 10% of test data which is a reasonable correlation for concept level analysis or quicker turnaround trade studies. Care should be taken for systems or load cases where the primary aberration is not de-spacing which may amplify this effect. These effects may be further examined in a future SBIR.

It is therefore recommended to maintain a fine mesh size using glued or merged nodes at adhesive interfaces and be aware of clear aperture size relative to element size. Using an element size that is too coarse will result in a higher percent of the displacement not fit by polynomials, which adds potential sources of error. The “percent not fit by polynomials” should always be reviewed, and the mesh size should be increased until the percent is acceptably small for the optic and load case in question. When applying the clear aperture within SigFit, the element size relative to the clear aperture may lead to inappropriate aperture shapes and will show the largest effect on the P-V where max/min values may not be retained due to excluding too many elements (most clearly seen in Trade #2d in Figure 4-10). This can be tuned using the parameter APERTOL as described further in Trade #3 below.

Trade	Description	WFE											
		0°C				40°C				0°C & 40°C Average			
		PV		RMS		PV		RMS		PV	RMS		
		[waves]	[nm]	[waves]	[nm]	[waves]	[nm]	[waves]	[nm]	[nm]	% Diff.	[nm]	% Diff.
Test Data		-	606	-	139	-	610	-	147	608	-	143	-
Pre-test		1.02550	520	0.28140	143	1.0139	514	0.2813	143	517	-15%	143	-0.2%
2ab	Solid Adhesive, glued on both sides	1.02560	520	0.28140	143	1.0140	514	0.2813	143	517	-15%	143	-0.2%
2c	Tet Adhesive, glued on both sides	1.02560	520	0.28140	143	1.0139	514	0.2813	143	517	-15%	143	-0.2%
2d	Tet Adhesive, Coarse Tet Optic, glued on both sides	1.02490	520	0.28130	143	1.0137	514	0.2811	143	517	-15%	143	-0.3%
2e	Tet Adhesive, Coarse Tet Optic w/ CA mesh split, glued on both sides	1.02420	519	0.28110	143	1.0139	514	0.2813	143	517	-15%	143	-0.3%
2f	Beam/spring Adhesive - no backfill, Coarse Tet Optic w/ CA mesh split	1.17400	595	0.30500	155	1.2001	609	0.3050	155	602	-1%	155	8.2%
2g	Beam/spring Adhesive - no backfill, Fine Brick Mesh with adhesive split	1.24760	633	0.31210	158	1.2356	627	0.3120	158	630	4%	158	10.7%

$\lambda = 5.07E-07$ m

% Difference < 2.0%
% Difference < 10.0%
% Difference > 10.0%

Table 4-3. Trade #2 WFE Values Comparison

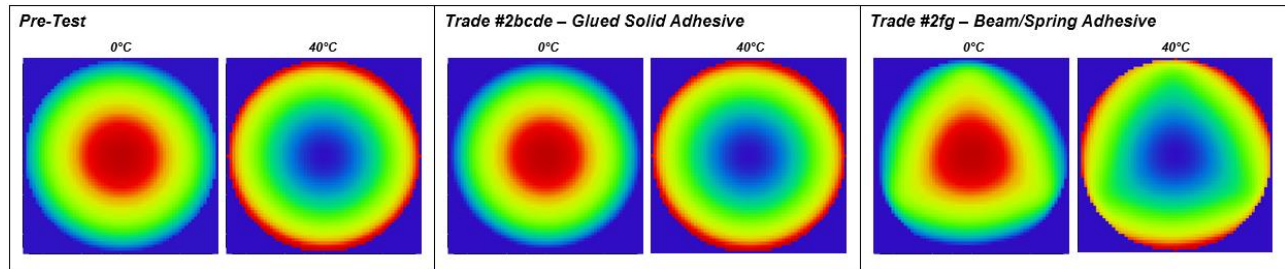


Figure 4-8. Trade #2 WFE Shape Comparison

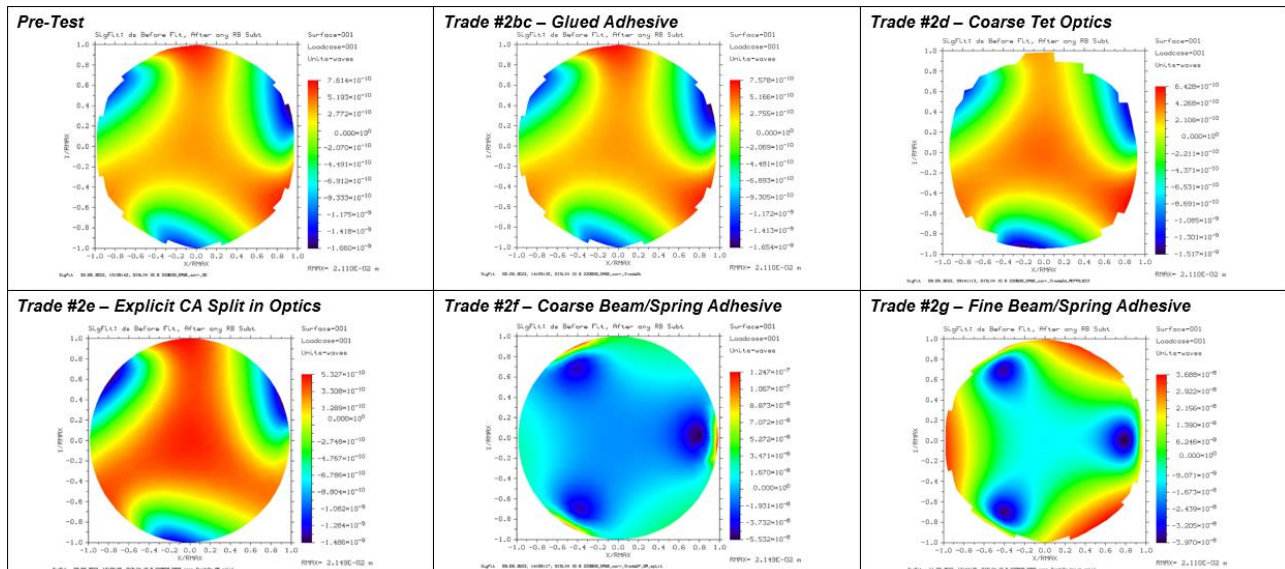


Figure 4-9. Trade #2 T1 Surface Figure Error Shapes

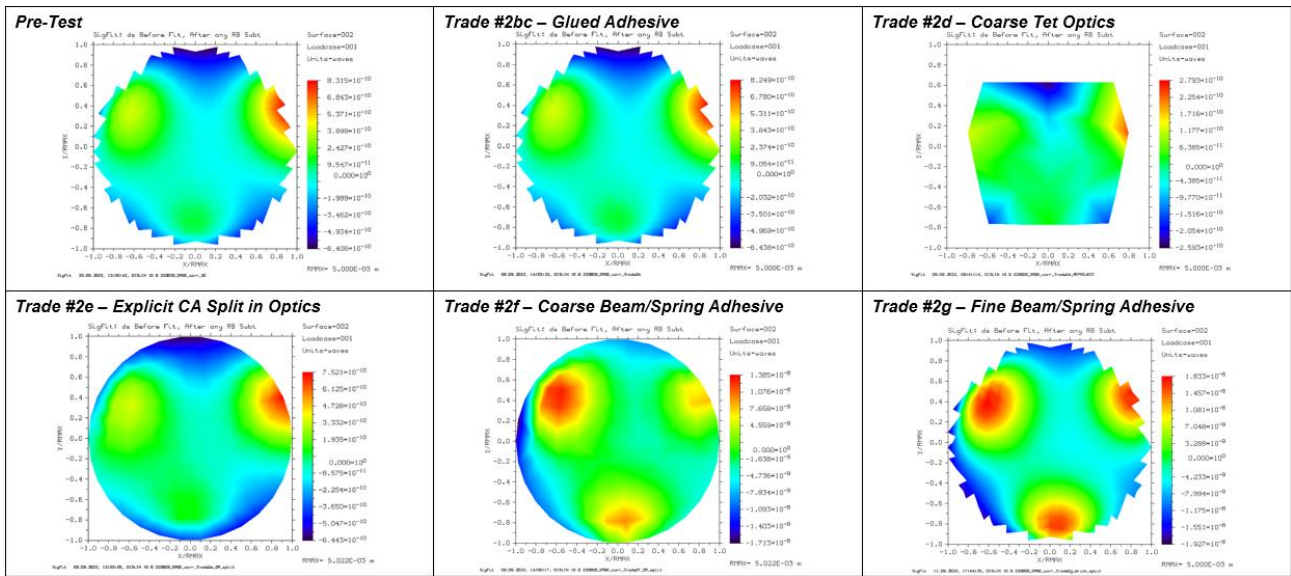


Figure 4-10. Trade #2 T2 Surface Figure Error Shapes

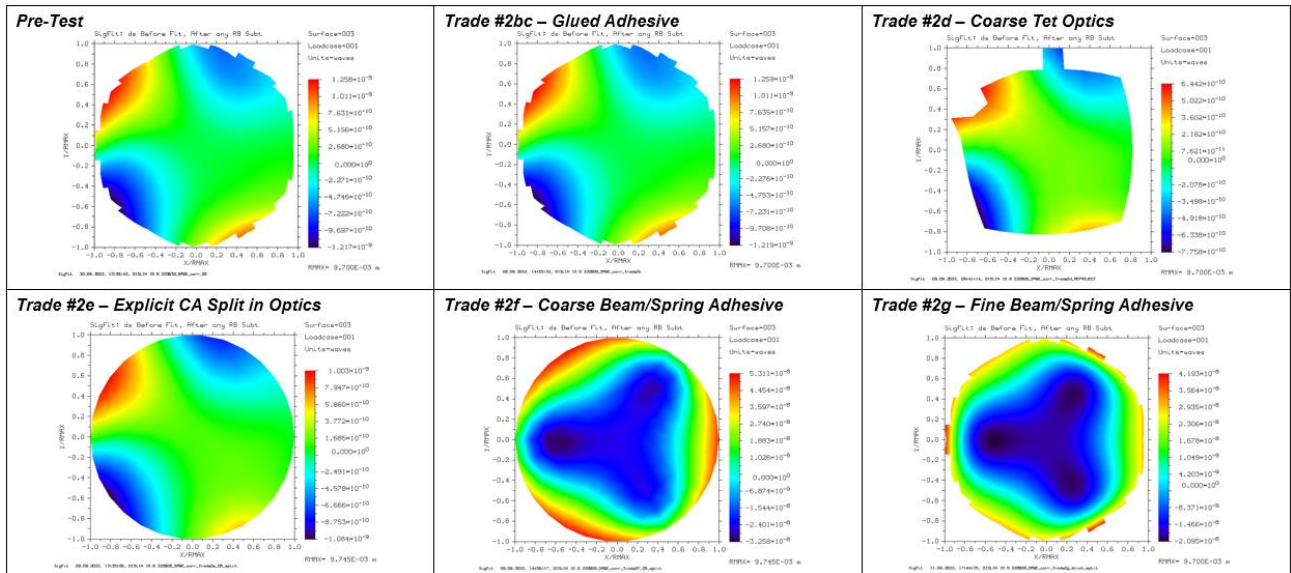


Figure 4-11. Trade #2 T3 Surface Figure Error Shapes

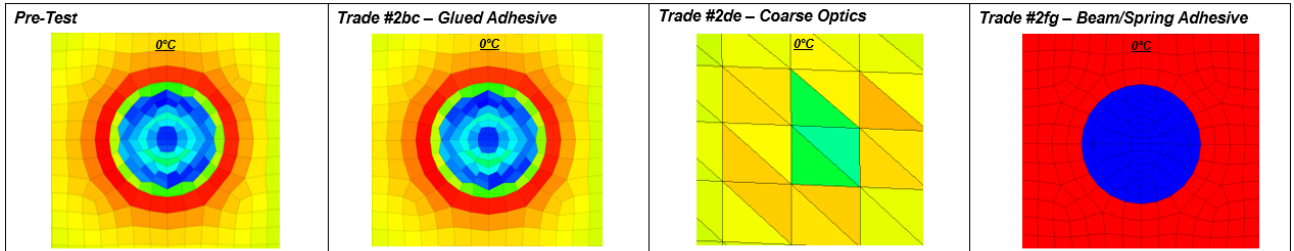
Stress results were very close when updating the adhesive joint to glued contact or using merged nodes, or when using brick or parabolic tetrahedral meshes – assuming the element size is consistent. Updating to coarse parabolic tetrahedral mesh on the glass optic greatly reduced optic stress, while updating to coarse parabolic tetrahedral mesh on the adhesive increased the adhesive stress. Either option should be used with caution for stress recovery, as expected. Stresses in the optics are summarized for all three optics in Table 4-4 and stress contours are shown in Figure 4-12 for T1 (T2 and T3 show similar contour trends). Stresses in the adhesives are summarized for all three optics in Table 4-5 and stress contours are shown in Figure 4-13 for T1 (T2 and T3 show similar contour trends). It is not recommended to recover stresses from either the optic or the mount from a FEM utilizing a beam/spring representation for the adhesive as the stresses increase dramatically.

Component	Material	Post-Processing Output Vector	Pre-test		Avg Trade #2bc		Avg Trade #2de		Avg Trade #2fg		Pre-test		Avg Trade #2bc		Avg Trade #2de		Avg Trade #2fg			
			0C	+40C	0C	+40C	0C	+40C	0C	+40C	0C	+40C	0C	+40C	0C	+40C	0C	+40C	0C	+40C
			Stress [Mpa]	Stress [Mpa]	Stress [Mpa]	Stress [Mpa]	Stress [Mpa]	Stress [Mpa]	Stress [Mpa]	Stress [Mpa]	Stress [Mpa]	Stress [Mpa]	Ultimate MS	Ultimate MS	Ultimate MS	Ultimate MS	Ultimate MS	Ultimate MS	Ultimate MS	Ultimate MS
T1 Optic	Zerodur	Max Prin/Shear	1.5	2.2	1.6	2.7	0.5	1.5	121.1	132.9	9.1	5.9	8.7	4.6	26.7	9.0	-0.9	-0.9		
T2 Optic	Zerodur	Max Prin/Shear	3.1	5.0	3.2	5.3	1.3	2.8	140.0	141.5	3.9	2.0	3.8	1.9	10.5	4.4	-0.9	-0.9		
T3 Optic	Zerodur	Max Prin/Shear	1.9	2.8	2.0	2.9	0.4	0.9	159.8	133.2	7.0	4.4	6.8	4.1	37.8	15.5	-0.9	-0.9		

¹ Glass margins utilize shellcoat Max Principal or Max Shear elemental w/o corner data, Adhesive margins utilize solid von Mises elemental w/ corner data for Hysol 9394 and solid Max Principal elemental w/ corner data for Zerodur

² MS includes ultimate SF of 1.4 for glass margins, and SF of 1.5 with an additional 1.25 uncertainty factor for optic-to-mount adhesive

Table 4-4. Trade #2 Optic Stress Comparison



*All contours are T1 (T2 & T3 show similar trend), contours set to max/min from Pre-test

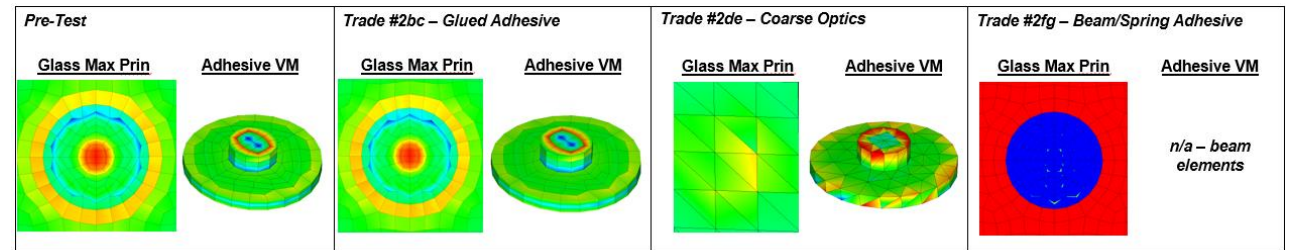
Figure 4-12. Trade #2 T1 Optic Stress Contour Comparison

Component	Material	Post-Processing Output Vector	Pre-test		Avg Trade #2bc		Avg Trade #2de		Avg Trade #2fg		Pre-test		Avg Trade #2bc		Avg Trade #2de		Avg Trade #2fg	
			0C	+40C	0C	+40C	0C	+40C	0C	+40C	0C	+40C	0C	+40C	0C	+40C	0C	+40C
			Stress [Mpa]	Stress [Mpa]	Stress [Mpa]	Stress [Mpa]	Stress [Mpa]	Stress [Mpa]	Stress [Mpa]	Stress [Mpa]	Stress [Mpa]	Stress [Mpa]	Ultimate MS	Ultimate MS	Ultimate MS	Ultimate MS	Ultimate MS	Ultimate MS
T1 Optic-to-Mount Adhesive	Hysol 9394	von Mises	19.7	19.7	22.1	22.1	26.8	26.8	-	-	3.4	3.4	2.9	2.9	2.3	2.3	-	-
	Zerodur	Max Prin	2.7	2.8	2.7	2.9	1.8	2.3	229.8	233.0	4.6	4.4	4.7	4.2	7.4	5.5	-0.9	-0.9
T2 Optic-to-Mount Adhesive	Hysol 9394	von Mises	18.4	18.4	20.1	20.1	34.1	34.1	-	-	5.6	5.6	5.0	5.0	2.6	2.6	-	-
	Zerodur	Max Prin	4.2	5.8	4.3	6.3	3.7	5.0	280.8	270.7	2.6	1.6	2.5	1.4	3.1	2.0	-0.9	-0.9
T3 Optic-to-Mount Adhesive	Hysol 9394	von Mises	20.8	20.8	23.3	23.3	25.4	25.4	-	-	3.7	3.7	3.2	3.2	2.9	2.9	-	-
	Zerodur	Max Prin	4.6	3.2	4.3	3.0	2.4	2.6	318.1	288.1	2.3	3.7	2.5	4.0	5.3	4.8	-1.0	-0.9

¹ Glass margins utilize shellcoat Max Principal or Max Shear elemental w/o corner data, Adhesive margins utilize solid von Mises elemental w/ corner data for Hysol 9394 and solid Max Principal elemental w/ corner data for Zerodur

² MS includes ultimate SF of 1.4 for glass margins, and SF of 1.5 with an additional 1.25 uncertainty factor for optic-to-mount adhesive

Table 4-5. Trade #2 Adhesive Stress Comparison



*All contours are T1 (T2 & T3 show similar trend), contours set to max/min from Pre-test

Figure 4-13. Trade #2 T1 Adhesive Stress Contour Comparison

4.3 Trade Study 3 Results

Trade #3 examined the effect of applying the clear aperture within SigFit versus via an explicit mesh split line as shown in Figure 4-14. WFE is shown to be nearly identical with either option – however, the same caveats as above apply that greater sensitivity in WFE is likely for systems with different load cases including temperature gradients across each optic.

The FEA area percent difference from Zemax varies greatly depending on the method of applying the clear aperture. As shown in Table 4-6, it is most accurate to explicitly split the mesh at the clear aperture regardless of element size. When applying the clear aperture in SigFit, the parameter APERTOL can be used to improve the nodes retained from FEM to more closely match the Zemax area and shape (see Figure 4-15). However, APERTOL is a relative tolerance that applies at the system level. It is recommended to aim to have a similar number of nodes across each optic diameter

for APERTOL to work most efficiently. However, attention should be given to the displacement expected at each optic and the mesh size should be chosen to appropriately capture the displacements as Zernike coefficients.

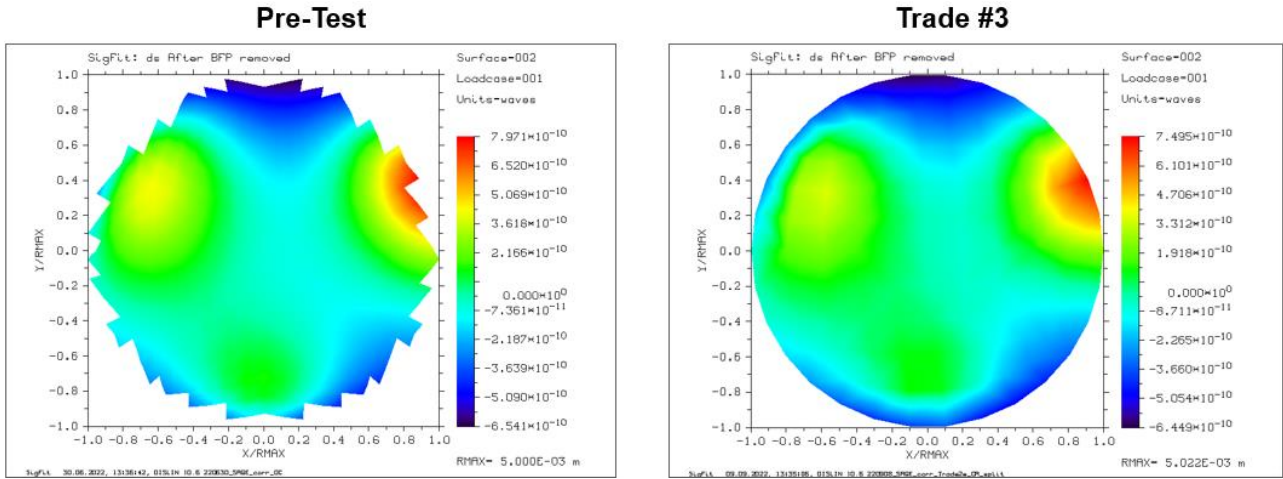


Figure 4-14. Clear Aperture Definition for Pre-test (left) and Trade #3 (right)

Trade	Method of Aperture	Optic Element Size	APERTOL	FEA Area [m ²]			% Difference from Zemax			
				T1	T2	T3	T1	T2	T3	
n/a	Zemax	-	-	1.45E-03	7.87E-05	2.96E-04	-	-	-	<p>Fine mesh – default APERTOL matches reasonably well</p> <p>Coarse mesh – need larger APERTOL to match larger optics, does NOT represent smaller T2 well</p> <p>Coarse mesh – need very large APERTOL to match smallest T2 optic, does NOT represent largest T1 well</p> <p>Explicit mesh split – best match!</p>
3a	Sigfit Area using applied Aperture	0.5mm	0.01	1.38E-03	7.11E-05	2.83E-04	5%	10%	5%	
3b		2mm	0.01	1.28E-03	4.94E-05	2.23E-04	12%	37%	25%	
3c		2mm	0.01	1.28E-03	4.94E-05	2.27E-04	11%	37%	24%	
3d		2mm	0.05	1.34E-03	4.94E-05	2.36E-04	7%	37%	20%	
3e		2mm	0.0625	1.38E-03	4.94E-05	2.47E-04	5%	37%	17%	
3f		2mm	0.075	1.41E-03	4.94E-05	2.60E-04	3%	37%	12%	
3g		2mm	0.1	1.46E-03	4.94E-05	2.74E-04	1%	37%	8%	
3h		2mm	0.125	1.50E-03	4.94E-05	2.85E-04	3%	37%	4%	
3i		2mm	0.2	1.54E-03	5.30E-05	3.09E-04	6%	33%	4%	
3j		2mm	0.25	1.62E-03	6.29E-05	3.26E-04	11%	20%	10%	
3k	2mm	0.275	1.69E-03	6.59E-05	3.24E-04	17%	16%	9%		
3l	2mm	0.3	1.80E-03	6.72E-05	3.26E-04	24%	15%	10%		
3m	2mm	0.32	1.80E-03	7.28E-05	3.28E-04	24%	8%	10%		
3o	2mm	0.35	1.80E-03	8.49E-05	3.28E-04	24%	8%	10%		
3p	2mm	0.5	1.7974E-03	9.38E-05	3.31E-04	24%	19%	12%		
3q	Explicit Mesh Split	2mm	-	1.4504E-03	7.87E-05	2.96E-04	0%	0%	0%	

Table 4-6. Trade #3 Parameters & Clear Aperture Area Comparison

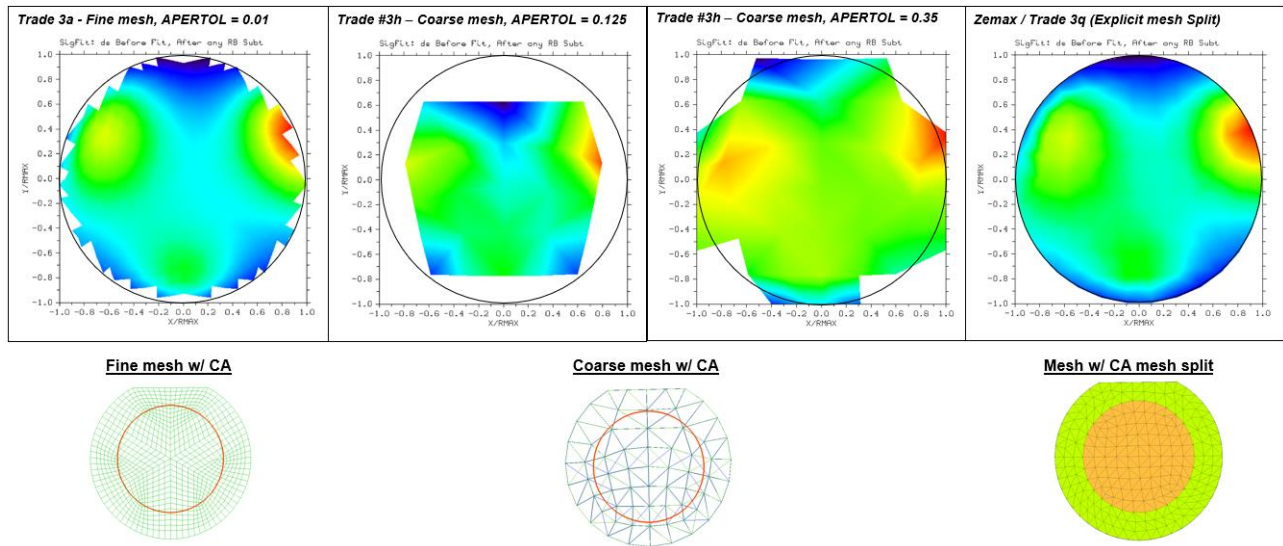


Figure 4-15. Trade #3 Clear Aperture Shape and Mesh Size Comparison

6. CONSIDERATIONS FOR FUTURE ANALYSIS & TESTING

There are several improvements and lessons learned for thermal testing of WFE that should be implemented in the future. These include use of a more permanent and verified air current blocker, monitoring clean room temperatures during testing to ensure stability of room temperature values (and ultimately stability of thermal chamber window WFE to be subtracted), and monitoring and/or extending temperature soak time before WFE is collected.

It is worth noting that the System Level Correlation assembly WFE under uniform thermal loading is driven primarily by de-spacing between optics due to the aluminum bench CTE. Different system designs or non-uniform temperature cases on the assembly may produce higher order aberrations that could be more sensitive to the modeling approaches discussed above. Care should be taken to not extrapolate these conclusions to different use cases. There is a need/desire for future development in additional types of loading (i.e. TVAC, non-uniform temperature loading), temperature loading to higher and lower temperatures (-40°C to +60°C), and in different types of optic mounting (preloaded flexures or retaining rings).

7. SUMMARY & CONCLUSION

The System Level Correlation assembly passed all test readiness review criteria for the Phase 1 thermal test (temperature range = 0°C to +40°C). At all temperatures between 0°C and +40°C, RMS WFE was <4.4% change from average WFE, where the target/objective was 5/10%. At 20°C (room temperature), the RMS WFE remained <7nm on average where <10nm is considered within the measurement resolution and noise floor. Additionally, the measured RMS WFE matches FEM predictions within 4% across the temperature range 0°-40°C, which exceeds the initial goal to correlate within 5-10% of FEA predictions.

Since the initial comparison of WFE test data to FEA predictions was already within the target set for the correlation (4% difference from FEM to test), the correlation effort focused on sensitivity of modeling approaches to improve efficiency while maintaining a low percent difference from FEA to test. These trade studies were targeted in three main areas: 1) Modeling of Liquid Pin Joint 2) Modeling of Optic and Optic-to-Mount Joint 3) Aperture Definition in FEM. Recommendations for each are provided in the sections above. Future work should include testing and comparison to pre-test analysis for additional optic mount designs and temperature load cases to further validate or update the recommendations provided in this paper.

ACKNOWLEDGEMENTS

The work associated with this paper is supported by NASA Langley Research Center and funded by the NASA SBIR office. Specific acknowledgement is due to the SAGE Principal Investigators Rob Damadeo and Charles Hill for their guidance, support, and review.

REFERENCES

- [1] Siemens PLM Software, NX/Nastran 11.0.2 (2017).
- [2] SigmaDyne SigFit 2020R1G, (2020).
- [3] Zemax Corporation, Zemax OpticStudio 18.9(2018).